THE JOURNAL OF PHYSICAL CHEMISTRY Letters

LETTER

pubs.acs.org/JPCL

Supercapacitor Capacitance Exhibits Oscillatory Behavior as a Function of Nanopore Size

Guang Feng[†] and Peter T. Cummings[*,†,‡]

[†]Department of Chemical and Biomolecular Engineering, Vanderbilt University, Nashville, Tennessee 37235, United States

[‡]Center for Nanophase Materials Sciences, Oak Ridge National Laboratory, Oak Ridge, Tennessee 37831, United States

Supporting Information

ABSTRACT: Supercapacitors composed of slit-shaped micropores ranging in size from 0.67 to 1.8 nm in a room-temperature ionic liquid were studied to investigate the dependence of capacitance (C) on the pore size (d) using molecular dynamics simulations. The capacitance versus pore size (i.e., the $C-d$ curve) was found to exhibit two peaks located at 0.7 and 1.4 nm, respectively. Specifically, as the pore shrinks from 1.0 to 0.7 nm, the capacitance of the micropore increases anomalously, in good agreement with experimental observations. We report herein that the second peak within 1.0 to 1.8 nm is a new feature of the $C-d$ curve. Furthermore, by analogy to the wave interference, we demonstrate that the interference of two electrical double layers near each slit wall does not only explain the entire $C-d$ curve, including the anomalous character, but also predicts the oscillatory behavior of $C-d$ curve beyond 1.8 nm.

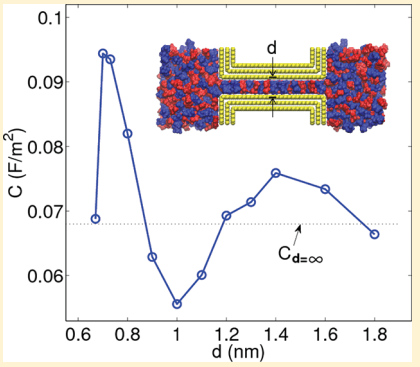

SECTION: Energy Conversion and Storage

Electrical energy storage plays a critical role in many high-profile energy technologies, such as the electric vehicles and generation of electricity from renewable sources. As a class of promising energy storage devices, electrical double-layer (EDL) capacitors, also called supercapacitors, have attracted considerable attention in electrical energy community.[1−4] To date, most studies have focused on addressing the limitation of supercapacitors related to their moderate energy density. One emerging direction for enhancing energy density has been the introduction of porous carbon-based materials as novel electrodes for supercapacitors, which, with their high specific surface area and good electrical conductivity, are able to improve the energy density.[3,5−9] By narrowing pores in carbon electrodes, experiments exhibited an anomalous increase in the area-normalized capacitance of micropores (<2 nm) with an organic electrolyte of tetraethylammonium tetrafluoroborate ([TEA][BF_4]) in the aprotic solvent acetonitrile (ACN).[10] Similar trends were reported at the same time by Raymundo-Piñero et al.[11] Lota et al.[12] found that the specific capacitance of activated carbon electrodes immersed in an aqueous electrolyte of 6 M KOH solution increases from ∼0.06 to ∼0.12 F/m^2 as the electrode pore size decreases from 1.45 to 1.06 nm. Largeot et al.[13] revealed that a sharp increase in capacitance occurs as the pore size decreases from 1.1 to 0.7 nm for micropores in a room-temperature ionic liquid (RTIL) 1-ethyl-3-methylimidazolium bis(trifluoromethylsulfonyl)imide ([emim][Tf_2N]); they emphasized that the maximum capacitance can be achieved at pore size of 0.7 nm, which is comparable to the ion size. Note that in Largeot et al.'s study, the pore size is actually averaged over a narrow unimodal pore size distribution on the carbon electrode.

Although this anomalous behavior of capacitance scaling has been ascribed to the distortion of the solvation shell of ions inside narrow pores with the presence of solvent,[10,14] the underlying physics of the capacitance of microporous carbon materials remains poorly understood, especially for the case of solvent-free electrolytes such as RTILs. Contrary to previous results,[10] a very recent experiment claimed that the specific capacitance in the same electrolyte ([TEA][BF_4]/ACN)[10] varies little as the pore size changes from 15 to 0.7 nm,[15] prompting the question: does the anomalous increase in capacitance with decreasing pore size actually exist? Several prior theoretical and simulation approaches have attempted to verify the existence of, and thus understand, the anomalous capacitance enhancement at small pore size. Examples include the electric wire-in-cylinder capacitor (EWCC) model[16] for cylindrical pores and the sandwich model[17] for slit-shaped pores, which have recently been proposed to rationalize the anomalous capacitance increase in micropores and provide a good fit to experimental data in the anomalous regime. On the basis of the mean-field theory and Monte Carlo simulations, Kornyshev et al.[18,19] suggested that the anomalous increase is attributed to the "superionic state" of ions inside pores arising from the image forces that exponentially screen out the electrostatic interactions of ions in the pore interior. However, this work considered the electrolyte ions as charged hard spheres, neglecting the van der Waals interactions and complex ionic structure that may play a role of the EDL

Received: September 27, 2011
Accepted: October 25, 2011
Published: October 25, 2011

inside micropores.[20] Molecular dynamics (MD) simulations overcome this restriction by modeling ions/molecules in atomistic chemical detail and have reproduced the capacitance scaling measured in experiments.[20,21] Compared with experiment, MD simulation is uniquely capable of leading to an understanding of the role of pore size in capacitance because the pore size can be fixed precisely in MD simulation, whereas in experiments the pore size is described by a distribution that in some cases can be quite broad or even multimodal. Particularly in the latter case, the term "average pore size" may not be meaningful. However, in previously reported MD simulations, either the range of pore sizes considered or the magnitude of capacitance departs significantly from experiments. For example, Shim et al.[20] performed MD simulations with the RTIL [emim][BF_4] as electrolyte and carbon nanotube (CNT) as the micropore. Although the capacitance was found to increase as the CNT diameter decreases from 2.03 to 0.95 nm, the overall specific capacitance is ~1 order of magnitude smaller than that observed experimentally. Pore geometry is probably one of the reasons responsible for this discrepancy because slit-shaped pores, rather than cylindrical ones, are thought to be more appropriate for the microporous carbon materials and graphene-based supercapacitors used in experiments.[13,22]

Despite these theoretical and modeling studies on the dependence of capacitance on pore size, the origin of the anomalous behavior below a critical pore size (~1 nm) is still not clear, nor is the role of EDLs in micropores. Furthermore, the EWCC and sandwich models are not suitable for relatively large micropores and mesopores. Finally, to rationalize the very different findings reported by Chmiola et al.[10] and Centeno et al.[15] aforementioned, the capacitance scaling for pores larger than that critical value needs to be studied. This regime has not been significantly considered previously, unlike the anomalous capacitance region.

Motivated by these considerations, we investigated the pore-size dependence of capacitance over a broad range of pore size, including the anomalous capacitance scaling, by performing MD simulations of EDLs inside micropores with an IL [emim]-[Tf_2N]. In the simulation system shown in Figure S1 of the accompanying Supporting Information (SI), the slit-shaped micropore[13] consists of two flat walls, and both of them were modeled by three graphene layers and separated by a center-to-center distance (the slit width, d) ranging from 0.67 to 1.8 nm. The surface charge density (σ) on the electrode surface was produced by assigning a small charge among the atoms on the graphene layers in contact with ILs and was tuned to generate a potential of ~2.82 V[23] between cathode and anode. In this Letter, we refer to the positively and negatively charged slits as the anode and cathode of the modeled supercapacitor, respectively. To satisfy the overall electroneutrality of the system, we immersed the cathode and anode, separated by a distance large enough to ensure bulk behavior between them, in IL bath. (See Figure S1 of the SI.) Details of the simulation model can be found in the SI. Additionally, simulations of EDLs in [emim][Tf_2N] near planar electrodes with open surface under different applied potentials were performed to provide a baseline for comparison.

We begin our analysis by examining the electric potentials in the IL bath and on the electrode. The potential in the center of IL bath (ϕ_{bath}) was found to be nearly independent of slit size; that is, $\phi_{bath} = 28.4 \pm 16.2$ mV. Also, the potential (ϕ) on the cathode and anode was measured by that in the center part of slit surface. (See Figure S1 of the SI.) Therefore, edge effects from the slit entrance are eliminated because the slit is long enough so that the electric potential varies only slightly in the center part of slit. (See Figure S2 of the SI.) With zero charge on the electrode, the potential drop between the electrode and IL bath, marked as the potential of zero charge (ϕ_{PZC}), was found to depend little on slit size; that is, $\phi_{PZC} = -0.04 \pm 0.03$ V. For charged electrodes, we observed that the magnitude of potential drop between the cathode and IL bath, with respect to ϕ_{PZC}, is quite close to that for the anode; that is, $|\phi_{cathode} - \phi_{bath} - \phi_{PZC}| \approx |\phi_{anode} - \phi_{bath} - \phi_{PZC}|$, which is ~1.41 V for slits explored in our simulations. This approximate symmetry arises from the similar size of $emim^+$ and Tf_2N^- ions.[13,23] Accordingly, the integral capacitance of each slit was calculated by $C = \sigma/(\phi - \phi_{bath} - \phi_{PZC})$.

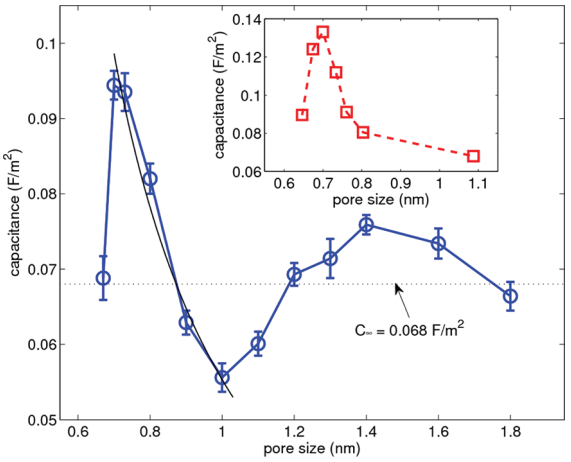

Figure 1. Specific capacitance of micropore as a function of pore size. The thick solid line connecting the circular symbols represents the MD simulation results reported in this work. The thin solid line without symbols is obtained from fitting eq 1 to the anomalous increase in capacitance with pore size ranging from 0.7 to 1.0 nm. The dashed line with square symbols, in the insert, represents the experimental data from ref 13.

The capacitance of micropore versus the pore size of slits studied, that is, the $C-d$ curve, is shown in Figure 1. We observe that the MD-generated $C-d$ curve has two peaks with maxima located at 0.7 and 1.4 nm, respectively. There are several noteworthy features of the MD-generated $C-d$ curve: (i) there is an anomalous increase in the capacitance as the slit shrinks from 1.0 to 0.7 nm, which is well consistent with that observed in experiments;[10,13,23] (ii) below 0.7 nm, the capacitance of micropore decreases with pore size, also consistent with experiments;[12,22] (iii) for pores greater than 1.0 nm, the capacitance increases to a maximum at 1.4 nm, and then decreases with the pore size increasing. The first peak on $C-d$ curve is in good accord with the experimental results (Figure 1),[13] except for its smaller magnitude. This difference possibly results from the use of nonpolarizable electrode surface and rigid graphene sheets modeled in MD simulations reported here: specifically, image forces arising from electrode polarization could lead to additional ion-electrode attractions and hence enable more ions of the same sort to occupy the pore,[19,24,25] and thus proper accounting of electronic polarizability may be needed for a more rigorously quantitative analysis; additionally, flexible carbon walls may also accommodate more ions entering the pore.[26] Interestingly, a second maximum peak of $C-d$ curve occurs within 1.0 to 1.8 nm, which is a new feature of the relation between the capacitance and pore size. This $C-d$ curve with multiple peaks could explain the absence of anomalous capacitance enhancement in the recent controversial experiment.[15] That is, the anomalous increase could be masked in a

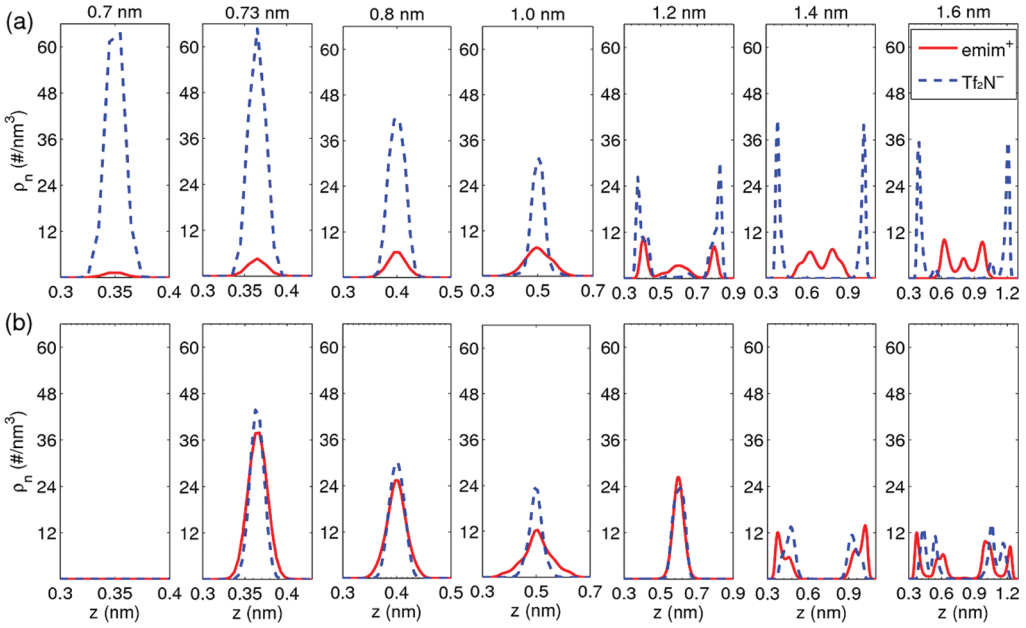

Figure 2. Number density profiles of ions across slit pores with various widths under (a) a potential of 1.41 V and (b) zero potential.

porous material with broad pore-size distribution because the measured capacitance is averaged over pore size. For example, if the pore size distribution was flat between 0.67 to 1.0 nm, then the corresponding capacitance averaged over that range is 0.076 F/m^2, which is only 11.8% larger than the capacitance for planar electrodes. Therefore, the accurate control of pore-size distribution in electrodes is crucial for characterizing the capacitive performance of supercapacitors.

To understand the behavior of the two peaks of $C-d$ curve, the microstructure of EDLs inside each micropore was explored by calculating the ion number density (ρ_n) based on the center of mass of ions across slit pore in Figure 2, in which $z = 0$ corresponds to the layer of graphene sheets in contact with ILs. (See Figure S1 of the SI.)

First, regardless of potentials applied, both cations and anions were found to accumulate primarily at the central plane of the slits with the size of 0.7 to 1.0 nm due to the confinement of slits. Hence, the narrower the slit, the closer the ions reside to the slit wall so that the effective EDL thickness inside slits becomes smaller, yielding a larger capacitance.[16,17] In previous work on nanoslits filled with aqueous electrolytes, a sandwich model was proposed to describe the anomalous enhancement of capacitance of nanoslit in which a counterion layer was located exactly midway between two slit walls.[17] Although ions here are more complicated than monatomic, based on the similar insight that counterions (companying with few co-ions) form a single layer at the central plane of slits,[16,17] we extend sandwich model for ILs as

$$C = \frac{\varepsilon_r \varepsilon_0}{(d - d_{ion})/2} \quad (1)$$

where ε_0 is the permittivity of vacuum, ε_r is the dielectric constant of ILs inside slit, and d_{ion} is the effective ion size along the direction perpendicular to the slit wall and is determined by the ion structure and its orientation inside pore. Indeed, the ions, viewed in MD simulations, reorientate with changing slit size. For example, over the range of pore sizes considered in this work, Tf_2N^- anions prefer to be perpendicular to the walls (i.e., the carbon−carbon vector is perpendicular to the walls) for large pores ($\geq$0.9 nm) and to be parallel to the walls and located at the central plane of the small slit pores ($\leq$0.8 nm). Fitting the simulation data (Figure 1) to eq 1 gives $\varepsilon_r = 2.13$, which is larger than the vacuum value of 1 and smaller than that of bulk ILs ($\sim$10).[27] The value of $d_{ion} = 0.32$ nm is consistent with the size of ions in [emim][Tf_2N].[28]

Second, with the pore size reduced below 0.73 nm, no cations or anions could access the slit interior without applying potentials. (See Figure 2b.) This implies that the energy barrier for ions entering a subnanometer pore starts to play an important role for EDLs inside pores.[29] As the energy barrier becomes competitive with the driving force from the applied potential, the capacitance of such pores would decrease (e.g., 0.67 nm wide slit, see Figure 1) due to diminished slit accessibility. Essentially, given the energy cost to reorientate themselves, ions could be driven into such small nanopores under an applied potential, which is consistent with the observations that the counterion peak becomes lower and the imidazolium rings of emim$^+$ ions are more parallel to the slit surface in 0.67 nm wide pore than those inside the 0.73 nm wide one. It could be expected that for small enough pore size no ions could enter the slit even under a large potential (e.g., working voltage) so that such nanopore does not contribute to the energy storage.

Third, as the pore size increases beyond 1.0 nm, multiple layers of ions, rather than a single layer, were mostly found in the slits (Figure 2a), so that the second peak, a new feature of $C-d$ curve, cannot be explained either by the sandwich model or directly by slit accessibility. To understand this behavior, we need to build another connection between the capacitance and microstructure of the EDL inside micropore.

The well-known phenomenon of wave interference in physics describes the situation when two waves superpose to form a resultant one, with regions of constructive (peaks coinciding with peaks) and destructive (peaks coinciding with troughs) interferences. Because alternating layering of cations and anions is a key feature of EDLs in ILs near the open surface of planar

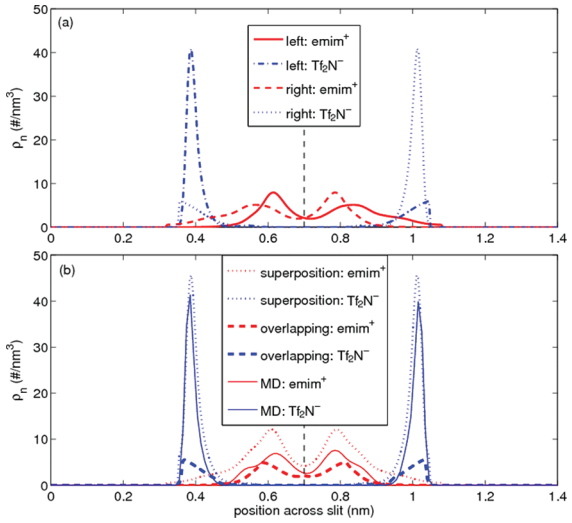

Figure 3. Interference of EDL structure: (a) superposition and (b) overlapping of ion number densities in a quasi-slit with size of 1.4 nm. The vertical black dashed line in each panel represents the center position at which the EDLs are symmetrized.

electrode,[30−35] the EDL at an open surface can be thought of as analogous to a spatially decaying wave, shown in Figure S3 of the SI. The spatially decaying "wave" is depicted by the number density distribution of ions in [emim][Tf_2N] near the planar graphene electrode under an applied potential of 1.41 V. When two parallel surfaces are involved, as in a slit pore, one could imagine that the EDL structure from each surface could interfere constructively or destructively. In this conceptual picture, the ion distribution in a slit pore can be considered to be the superposition of the ion distributions near the two open surfaces, placed symmetrically around the slit center.

Figure 3a illustrates the concept of EDL interference for a slit of size d = 1.4 nm. Where an EDL, obtained from the open surface under a potential of 1.41 V (Figure S3 of the SI), was shown with its symmetry (the same EDL symmetrized at a location of $d/2$), by plotting $\rho_n(z)$ and $\rho_n(d-z)$ both within the regime of $0 < z < d$ and truncated at each side due to the wall confinement. Then, the superposition prediction for the resultant EDL structure inside a slit, represented by ρ_n^S, is obtained by superposing the number density for the open interface, that is, $\rho_n^S(z) = \rho_n(z) + \rho_n(d-z)$, as shown in Figure 3b. As can be seen, the superposition-predicted EDL structure in the 1.4 nm wide slit is similar with that computed directly from MD simulation. The difference of their magnitude could be caused by the slit confinement and the charge overscreeing[30,36] that make the net charge in the first counterion and co-ion layer under-balance the counter-charge on the electrode surface. An additional quantity (ρ_n^O), defined by $\rho_n^O(z) = \min[\rho_n(z),\rho_n(d-z)]$, was used to characterize the overlapping part of two EDLs via their interference (Figure 3b). The superposition and overlapping of EDLs near two opposing walls to form a quasi-slit with various sizes are shown in Figures S4 and S5 of the SI. To quantify the interference effects on EDLs inside quasi-slit, we introduce an EDL interference factor as

$$f_I(d) = \int_0^d \rho_n^O(z)\,dz \Big/ \int_0^d \rho_n^S(z)\,dz \qquad (2)$$

The interference factor (f_I) for quasi-slits with sizes of 1.0, 1.2, 1.4, and 1.6 nm was calculated to be 0.019, 0.136, 0.230, and 0.143,

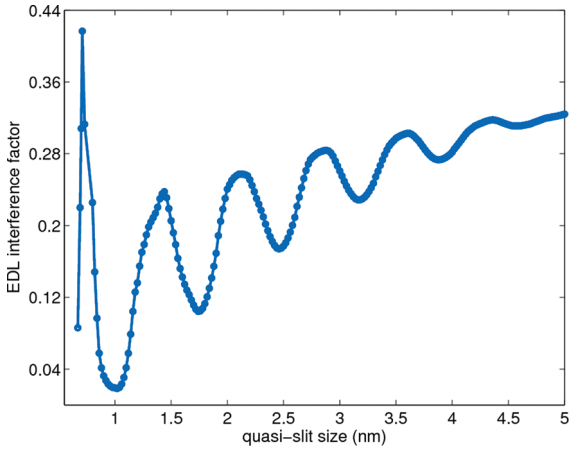

Figure 4. EDL interference factor as a function of quasi-slit size.

which has the same trend of the second peak on $C-d$ curve (Figure 1). The larger f_I at 1.4 nm results from the constructive interference by the peaks of cations and anions (Figure 3), and smaller values can be attributed to the destructive interference arising from the minima of ion distributions. This suggests that, as ions enter a slit pore under an applied potential, two EDLs originating from each slit wall would interfere with each other to form a resultant one. The larger f_I indicates that more ions could pack into the slit by the constructive interference, evidenced by the height of ion peaks in Figure 2a, which would cause the enhancement in the capacitance of micropore. On the contrary, destructive interference could reduce the capacitance by lessening the ion packing inside micropores.

Notice that the second peak on the $C-d$ curve has smaller amplitude than the first one. Taking the capacitance of EDLs near open surface (C_∞ = 0.068 F/m^2, Figure 1) as the reference, one can anticipate that the $C-d$ curve might have more peaks following the second one and damp eventually to the reference capacitance with further increasing pore size. For perspective, we calculated the interference factors for EDLs inside quasi-slits with size ranging from 0.67 to 5 nm, as shown in Figure 4. The locations of the first to fifth peaks are 0.71, 1.44, 2.12, 2.82, and 3.60 nm, whereas troughs are at 1.02, 1.74, 2.45, 3.18, and 3.88 nm. The curve of EDL interference factor within 0.67 to 1.8 nm has almost the same oscillatory behavior as the entire $C-d$ curve shown in Figure 1, that is, nearly the same locations of peaks or valleys on both curves, which further confirms that EDL interference plays a critical role in the relation between capacitance of a micropore and its size. Additionally, the EDL interference factors in Figure 4 suggest that (i) beyond 1.8 nm, the oscillatory behavior still exists but becomes less defined with pore size increasing; (ii) beyond ~4.5 nm, the oscillation is quite weak in magnitude. This suggests that (1) the $C-d$ curve may also have other peaks beyond 1.8 nm and would oscillate decreasingly toward 0.068 F/m^2 (Figure 1); (2) beyond ~4.5 nm, the capacitance would be almost the same as that for open surface electrode. Therefore, the EDL interference factor curve in Figure 4 provides a prediction of the oscillatory behavior of the $C-d$ curve (with almost the same locations of peaks and valleys as interference factor curve) in a quite wide range of pore size so that one can precisely control the pore to reach the optimal size and then achieve the optimized capacitance as well as the energy density of a supercapacitor, based solely on the EDL structure

near open surface under a similar potential. Moreover, the interference factor, calculated by taking different EDLs under potentials within 1.16 to 1.51 V, varies weakly with the applied potential because EDL structures, especially of the counterions, near open surface change little over this range of potential. (See the Figure S6 of the SI.) The distance between two adjoining peaks or troughs was found to be ∼0.7 nm, which is similar to the ion size. This implies that the ion size is a key of the curve of EDL interference factor in Figure 4 as well as the $C-d$ curve in Figure 1.

In summary, we performed MD simulations of a model supercapacitor with slit-shaped micropores in the IL [emim]-[Tf_2N] to characterize the relation between the capacitance and pore size. The $C-d$ curve exhibits two peaks at 0.7 and 1.4 nm, respectively. Specifically, with the pore size varying from 1.0 to 0.7 nm, the anomalous capacitance increase observed in our MD simulations agrees well with experimental findings. Below 0.7 nm, the capacitance decreases with the pore size, which is also consistent with the experiments. For pore size in the range 1.0 to 1.8 nm, we find a new feature of the $C-d$ curve, namely, second peak, which is observed for the first time in this work and suggests that the $C-d$ curve may be oscillatory. This multiple peak behavior of the $C-d$ curve offers a possible explanation for the capacitance nearly independent of pore size, as suggested by recent experiment:[15] this conclusion could result from the use of microporous electrodes with a broad pore-size distribution. Furthermore, analogized with the wave interference, the concept of EDL interference was introduced and found not only to account for the two-peak property of $C-d$ curve within 0.67 to 1.8 nm but also to predict that the $C-d$ curve could have more peaks above 1.8 nm. The picture that emerges is that the $C-d$ curve will exhibit oscillatory behavior as a function of pore size, eventually (at ∼4.5 nm) damping to the capacitance of EDLs near open surface. The oscillatory behavior of $C-d$ curve could provide a new point of view to optimize the pore size of electrodes as well as the energy density of a supercapacitor, simply based on knowledge of EDL structure near an open-surface electrode. Despite the absence of solvent in this work, the EDL interference concept may also work for aqueous electrolytes and organic electrolytes; additional work will be needed to verify this.

■ ASSOCIATED CONTENT

Ⓢ Supporting Information. Details of simulation model and the microstructures of electrical double layers in ionic liquids. This material is available free of charge via the Internet at http://pubs.acs.org.

■ AUTHOR INFORMATION

Corresponding Author

*E-mail: peter.cummings@vanderbilt.edu.

■ ACKNOWLEDGMENT

This work was supported as part of the Fluid Interface Reactions, Structures and Transport (FIRST) Center, an Energy Frontier Research Center funded by the U.S. Department of Energy, Office of Science, Office of Basic Energy Sciences, under award number ERKCC61. We appreciate the Palmetto cluster at Clemson University and the National Energy Research Scientific Computing Center for providing computer time.

■ REFERENCES

(1) Conway, B. E. *Electrochemical Supercapacitors: Scientific Fundamentals and Technological Applications*; Kluwer Academic/Plenum Publishers: New York, 1999.

(2) Christen, T.; Ohler, C. Optimizing Energy Storage Devices Using Ragone Plots. *J. Power Sources* **2002**, *110*, 107–116.

(3) Simon, P.; Gogotsi, Y. Materials for Electrochemical Capacitors. *Nat. Mater.* **2008**, *7*, 845–854.

(4) Burke, A. R&D Considerations for the Performance and Application of Electrochemical Capacitors. *Electrochim. Acta* **2007**, *53*, 1083–1091.

(5) Zhang, L. L.; Zhao, X. S. Carbon-Based Materials as Supercapacitor Electrodes. *Chem. Soc. Rev.* **2009**, *38*, 2520–2531.

(6) Lee, J.; Kim, J.; Hyeon, T. Recent Progress in the Synthesis of Porous Carbon Materials. *Adv. Mater.* **2006**, *18*, 2073–2094.

(7) Liang, C.; Li, Z.; Dai, S. Mesoporous Carbon Materials: Synthesis and Modification. *Angew. Chem., Int. Ed.* **2008**, *47*, 3696–3717.

(8) Dash, R.; Chmiola, J.; Yushin, G.; Gogotsi, Y.; Laudisio, G.; Singer, J.; Fischer, J.; Kucheyev, S. Titanium Carbide Derived Nanoporous Carbon for Energy-Related Applications. *Carbon* **2006**, *44*, 2489–2497.

(9) Frackowiak, E. Carbon Materials for Supercapacitor Application. *Phys. Chem. Chem. Phys.* **2007**, *9*, 1774–1785.

(10) Chmiola, J.; Yushin, G.; Gogotsi, Y.; Portet, C.; Simon, P.; Taberna, P. L. Anomalous Increase in Carbon at Pore Sizes Less Than 1 Nanometer. *Science* **2006**, *313*, 1760–1763.

(11) Raymundo-Piñero, E.; Kierzek, K.; Machnikowski, J.; Béguin, F. Relationship between the Nanoporous Texture of Activated Carbons and Their Capacitance Properties in Different Electrolytes. *Carbon* **2006**, *44*, 2498–2507.

(12) Lota, G.; Centeno, T. A.; Frackowiak, E.; Stoeckli, F. Improvement of the Structural and Chemical Properties of a Commercial Activated Carbon for Its Application in Electrochemical Capacitors. *Electrochim. Acta* **2008**, *53*, 2210–2216.

(13) Largeot, C.; Portet, C.; Chmiola, J.; Taberna, P.-L.; Gogotsi, Y.; Simon, P. Relation between the Ion Size and Pore Size for an Electric Double-Layer Capacitor. *J. Am. Chem. Soc.* **2008**, *130*, 2730–2731.

(14) Chmiola, J.; Largeot, C.; Taberna, P. L.; Simon, P.; Gogotsi, Y. Desolvation of Ions in Subnanometer Pores and Its Effect on Capacitance and Double-Layer Theory. *Angew. Chem., Int. Ed.* **2008**, *47*, 3392–3395.

(15) Centeno, T. A.; Sereda, O.; Stoeckli, F. Capacitance in Carbon Pores of 0.7 to 15 nm: A Regular Pattern. *Phys. Chem. Chem. Phys.* **2011**, *13*, 12403–12406.

(16) Huang, J.; Sumpter, B. G.; Meunier, V. A Universal Model for Nanoporous Carbon Supercapacitors Applicable to Diverse Pore Regimes, Carbon Materials, and Electrolytes. *Chem.—Eur. J.* **2008**, *14*, 6614–6626.

(17) Feng, G.; Qiao, R.; Huang, J.; Sumpter, B. G.; Meunier, V. Ion Distribution in Electrified Micropores and Its Role in the Anomalous Enhancement of Capacitance. *ACS Nano* **2010**, *4*, 2382–2390.

(18) Kondrat, S.; Kornyshev, A. A. Superionic State in Double-Layer Capacitors with Nanoporous Electrodes. *J. Phys.: Condens. Matter* **2011**, *23*, 022201.

(19) Kondrat, S.; Georgi, N.; Fedorov, M. V.; Kornyshev, A. A. A Superionic State in Nano-Porous Double-Layer Capacitors: Insights from Monte Carlo Simulations. *Phys. Chem. Chem. Phys.* **2011**, *13*, 11359–11366.

(20) Shim, Y.; Kim, H. J. Nanoporous Carbon Supercapacitors in an Ionic Liquid: A Computer Simulation Study. *ACS Nano* **2010**, *4*, 2345–2355.

(21) Yang, L.; Fishbine, B. H.; Migliori, A.; Pratt, L. R. Molecular Simulation of Electric Double-Layer Capacitors Based on Carbon Nanotube Forests. *J. Am. Chem. Soc.* **2009**, *131*, 12373–12376.

(22) Stoller, M. D.; Park, S.; Zhu, Y.; An, J.; Ruoff, R. S. Graphene-Based Ultracapacitors. *Nano Lett.* **2008**, *8*, 3498–3502.

(23) Lin, R.; Huang, P.; Ségalini, J.; Largeot, C.; Taberna, P. L.; Chmiola, J.; Gogotsi, Y.; Simon, P. Solvent Effect on the Ion Adsorption

from Ionic Liquid Electrolyte into Sub-Nanometer Carbon Pores. *Electrochim. Acta* **2009**, *54*, 7025–7032.

(24) Yan, T.; Burnham, C. J.; Del Pópolo, M. G.; Voth, G. A. Molecular Dynamics Simulation of Ionic Liquids: The Effect of Electronic Polarizability. *J. Phys. Chem. B* **2004**, *108*, 11877–11881.

(25) Outhwaite, C. W.; Lamperski, S.; Bhuiyan, L. B. Influence of Electrode Polarization on the Capacitance of an Electric Double Layer at and around Zero Surface Charge. *Mol. Phys.* **2010**, *109*, 21–26.

(26) Wander, M. C. F.; Shuford, K. L. Molecular Dynamics Study of Interfacial Confinement Effects of Aqueous NaCl Brines in Nanoporous Carbon. *J. Phys. Chem. C* **2010**, *114*, 20539–20546.

(27) Weingärtner, H. The Static Dielectric Constant of Ionic Liquids. *Z. Phys. Chem.* **2006**, *220*, 1395–1405.

(28) Perkin, S.; Crowhurst, L.; Niedermeyer, H.; Welton, T.; Smith, A. M.; Gosvami, N. N. Self-Assembly in the Electrical Double Layer of Ionic Liquids. *Chem. Commun.* **2011**, *47*, 6572–6574.

(29) Feng, G.; Qiao, R.; Huang, J.; Sumpter, B. G.; Meunier, V. Atomistic Insight on the Charging Energetics in Subnanometer Pore Supercapacitors. *J. Phys. Chem. C* **2010**, *114*, 18012–18016.

(30) Feng, G.; Qiao, R.; Huang, J.; Dai, S.; Sumpter, B. G.; Meunier, V. The Importance of Ion Size and Electrode Curvature on Electrical Double Layers in Ionic Liquids. *Phys. Chem. Chem. Phys.* **2011**, *13*, 1152–1161.

(31) Wang, S.; Li, S.; Cao, Z.; Yan, T. Molecular Dynamic Simulations of Ionic Liquids at Graphite Surface. *J. Phys. Chem. C* **2010**, *114*, 990–995.

(32) Vatamanu, J.; Borodin, O.; Smith, G. D. Molecular Simulations of the Electric Double Layer Structure, Differential Capacitance, and Charging Kinetics for *N*-Methyl-*N*-propylpyrrolidinium Bis(fluorosulfonyl)Imide at Graphite Electrodes. *J. Phys. Chem. B* **2011**, *115*, 3073–3084.

(33) Vatamanu, J.; Borodin, O.; Smith, G. D. Molecular Insights into the Potential and Temperature Dependences of the Differential Capacitance of a Room-Temperature Ionic Liquid at Graphite Electrodes. *J. Am. Chem. Soc.* **2010**, *132*, 14825–14833.

(34) Israelachvili, J. N. *Intermolecular and Surface Forces*, 2nd ed.; Academic Press: New York, 1992.

(35) Pinilla, C.; Del Pópolo, M. G.; Kohanoff, J.; Lynden-Bell, R. M. Polarization Relaxation in an Ionic Liquid Confined between Electrified Walls. *J. Phys. Chem. B* **2007**, *111*, 4877–4884.

(36) Kornyshev, A. A. Double-Layer in Ionic Liquids: Paradigm Change? *J Phys. Chem. B* **2007**, *111*, 5545–5557.